RESEARCH ARTICLE

JBMR®

Characterization of Extracellular Vesicles in Osteoporotic Patients Compared to Osteopenic and Healthy Controls

Jessica Pepe,[1#] Michela Rossi,[2#] Giulia Battafarano,[2] Pamela Vernocchi,[3] Federica Conte,[4] Valeria Marzano,[3] Eda Mariani,[5] Stefano Levi Mortera,[3] Cristiana Cipriani,[1] Ippolita Rana,[6] Paola Sabrina Buonuomo,[6] Andrea Bartuli,[6] Viviana De Martino,[1] Simone Pelle,[7] Luisa Pascucci,[8] Renato Maria Toniolo,[9] Lorenza Putignani,[10] Salvatore Minisola,[1#] and Andrea Del Fattore[2#]

[1]Department of Clinical, Internal, Anesthesiological and Cardiovascular Sciences, Sapienza University, Rome, Italy
[2]Bone Physiopathology Research Unit, Genetics and Rare Diseases Research Division, Bambino Gesù Children's Hospital, IRCCS, Rome, Italy
[3]Unit of Human Microbiome, Multimodal Laboratory Medicine Research Area, Bambino Gesù Children's Hospital, IRCCS, Rome, Italy
[4]Institute for System Analysis and Computer Science "A.Ruberti", National Research Council (CNR), Rome, Italy
[5]Research Laboratory, Bambino Gesù Children's Hospital, IRCCS, Rome, Italy
[6]Rare Diseases and Medical Genetic Unit, Bambino Gesù Children's Hospital, IRCCS, Rome, Italy
[7]"Polo Sanitario San Feliciano - Villa Aurora" Clinic, Rome, Italy
[8]Department of Veterinary Medicine, University of Perugia, Perugia, Italy
[9]Department of Orthopaedics and Traumatology, Bambino Gesù Children's Hospital, IRCCS, Rome, Italy
[10]Department of Diagnostics and Laboratory Medicine, Unit of Microbiology and Diagnostic Immunology, Unit of Microbiomics, and Multimodal Laboratory Medicine Research Area, Unit of Human Microbiome, Bambino Gesù Children's Hospital, IRCCS, Rome, Italy

ABSTRACT

Extracellular vesicles (EVs) are mediators of a range of pathological conditions. However, their role in bone loss disease has not been well understood. In this study we characterized plasma EVs of 54 osteoporotic (OP) postmenopausal women compared to 48 osteopenic (OPN) and 44 healthy controls (CN), and we investigated their effects on osteoclasts and osteoblasts. We found no differences between the three groups in terms of anthropometric measurements and biochemical evaluation of serum calcium, phosphate, creatinine, PTH, 25-hydroxy vitamin D and bone biomarkers, except for an increase of CTX level in OP group. FACS analysis revealed that OP patients presented a significantly increased number of EVs and RANKL$^+$ EVs compared with both CN and OPN subjects. Total EVs are negatively associated with the lumbar spine T-score and femoral neck T-score. Only in the OPN patients we observed a positive association between the total number of EVs and RANKL$^+$ EVs with the serum RANKL. In vitro studies revealed that OP EVs supported osteoclastogenesis of healthy donor peripheral blood mononuclear cells at the same level observed following RANKL and M-CSF treatment, reduced the ability of mesenchymal stem cells to differentiate into osteoblasts, while inducing an increase of *OSTERIX* and *RANKL* expression in mature osteoblasts. The analysis of miRNome revealed that miR-1246 and miR-1224-5p were the most upregulated and downregulated in OP EVs; the modulated EV-miRNAs in OP and OPN compared to CN are related to osteoclast differentiation, interleukin-13 production and regulation of canonical WNT pathway. A proteomic comparison between OPN and CN EVs evidenced a decrease in fibrinogen, vitronectin, and clusterin and an increase in coagulation factors and apolipoprotein, which was also upregulated in OP EVs. Interestingly, an increase in RANKL$^+$ EVs and exosomal miR-1246 was also observed in samples from patients affected by Gorham-Stout disease, suggesting that EVs could be good candidate as bone loss disease biomarkers. © 2022 The Authors. *Journal of Bone and Mineral Research* published by Wiley Periodicals LLC on behalf of American Society for Bone and Mineral Research (ASBMR).

KEY WORDS: MICROVESICLES; OSTEOPOROSIS; MIRNA; PROTEOMIC ANALYSIS; OSTEOCLAST

Received in original form March 19, 2022; revised form August 16, 2022; accepted August 24, 2022.
Address correspondence to: Salvatore Minisola, MD, Department of Clinical, Internal, Anesthesiological and Cardiovascular Sciences, "Sapienza" University of Rome, Rome 00185, Italy. E-mail: salvatore.minisola@uniroma1.it
Additional Supporting Information may be found in the online version of this article.
[#]Equal contributors.

Journal of Bone and Mineral Research, Vol. 37, No. 11, November 2022, pp 2186–2200.
DOI: 10.1002/jbmr.4688

Introduction

Although initially considered inert cellular debris, cell-derived membrane-enclosed vesicles, or extracellular vesicles (EVs), are increasingly recognized as playing a pivotal role in cell-to-cell communication.[1,2] EVs represent a heterogeneous population that includes exosomes and microvesicles that differ in size, origin, and antigenic composition. Exosomes are 40–100 nm in size, derived from multivesicular bodies (MVBs), and secreted via their fusion with the plasma membrane. Shedding vesicles, also known as microvesicles, are a heterogeneous population of membrane vesicles up to 1 μm in size directly derived from the cell membrane of activated cells through the disruption of the cortical cytoskeleton.[3,4] They are released by many cells, including cancer cells, immune cells, platelets, mesenchymal stem cells (MSCs), osteoclasts, and osteoblasts.[5,6] EVs may directly stimulate target cells by receptor-mediated interactions, or they may transfer ligands, receptors, proteins, DNA, mRNA, microRNA, and intact organelles (e.g., mitochondria) to target cells[3]; for these reasons, they have been studied as new diagnostic, prognostic or therapeutic tools in several diseases.[7,8]

Regarding bone metabolism, Huynh et al. demonstrated that osteoclast precursors released EVs that stimulate osteoclastogenesis; however, EVs secreted by mature osteoclasts inhibited the formation of mature osteoclasts, suggesting that EVs could act as regulators of bone remodeling activity.[9] Moreover, the proteomic characterization of vesicles released by osteoblasts identified proteins important for exosome biogenesis, formation, uptake, and osteogenesis.[10]

Although recent reports indicated the involvement of bone-associated EVs in the regulation of bone remodeling and bone diseases,[11-13] many processes remain unclear and are under investigation. So far, the analysis of both miRNA and proteomic content of EVs in postmenopausal women compared to osteopenic (OPN) and controls has never been described. The aim of this study was to characterize circulating EVs of osteoporotic (OP) patients compared to OPN and healthy controls (CN) and to investigate their effects on osteoclasts and osteoblasts.

Materials and Methods

Patients

One hundred two postmenopausal women (age range 50–85 years) were enrolled—54 OP patients and 48 OPN subjects—at the Mineral Metabolism Centre of the University of Rome "Sapienza" (Italy) from 2018–2021. Meanwhile, 44 healthy age-matched postmenopausal women with BMD T-score > −1.0 SD were enrolled as the control group (CN). The study was approved by the Umberto I Hospital Ethics Committee (Protocol No. 4524). Radiological examination methods and serum bone biomarkers are described in the Supplementary Materials. Exclusion criteria were as follows: estimated creatine clearance <60 mL/min, tumors, hepatitis C virus or hepatitis B virus co-infection and BMI >30 kg/m^2. In addition, none of the patients should have been previously treated with bone active drugs or with any treatments that could interfere with bone mineral metabolism (steroids, diuretics, thyroid hormones, anticonvulsant drugs, and lithium). Furthermore, no patients reported a history of known secondary osteoporosis. For the study of Gorham-Stout disease (GSD), 10 patients [the median age at diagnosis was 7.6 years (range 1 month to 25 years)] were recruited by the Rare Diseases and Medical Genetics Unit of Bambino Gesù Children's Hospital (OPBG). Informed consent was obtained by parents/legal guardians. The study was approved by OPBG's ethics committee (Protocol No. GR-2019-12370244, 01/02/2021). The diagnosis of GSD was based on radiological assessment and bone histology. The clinical description of the GSD patients was recently published in Rossi et al.[14] Fifteen control subjects were matched for age and gender and tested for standard serum markers to exclude inflammatory status.

Isolation of EVs

Circulating EVs were isolated from EDTA blood samples by centrifugation and ultracentrifugation methods.[15] In particular, samples were centrifuged at 1000*g* for 10 minutes and then at 4500*g* for 15 minutes at 10°C to remove platelets. The supernatant was diluted in PBS in polyallomer tubes, then ultracentrifuged at 100,000*g* at 4°C for 1 hour. At the end of the procedure, the supernatant was discarded and the pellet of EVs was resuspended in a proportional amount of PBS based on the volume of ultracentrifuged plasma.

Electron microscopy examination of EVs

EVs were morphologically evaluated by transmission electron microscopy (TEM). Several drops of EV suspension (about 20 μL each) were placed on Parafilm (Bemis, Neenah, WI, USA). Formvar-coated copper grids (Electron Microscopy Sciences, Hatfield, PA, USA) were placed over them, in a moist chamber, for 30 minutes at room temperature. Grids were then washed once in 0.1 M phosphate buffer (Sigma-Aldrich, St. Louis, MO, USA), pH 7.3, and twice in distilled water. Finally, they were contrasted with 2% uranyl acetate (Electron Microscopy Sciences, Hatfield, PA, USA), air dried, and observed under a Philips EM 208 transmission electron microscope equipped with a digital camera (University Centre for Electron Microscopy, CUME, Perugia, Italy).

FACS analysis of EVs

For FACS analysis, EVs were loaded with 2 μM carboxyfluorescein succinimidyl ester (CFSE) (Life Technologies, Carlsbad, CA, USA) and 1 μM PKH26 (Sigma-Aldrich) dyes, according to the manufacturer's instructions, to analyze the amount of EVs in each sample. We used commercial standard nanobeads (Sperotech, Inc., Lake Forest, IL, USA) in sizes of 1.3, 0.7 and 0.5 μm to create a dimensional gate of EVs. To evaluate the membrane expression of RANKL, EVs were incubated with a phycoerythrin (PE)-conjugated anti-RANKL antibody (BD Biosciences, San Jose, CA, USA) for 20 minutes at 4°C, then were analyzed by flow cytometry. Moreover, CountBright™ Absolute Counting Beads (Thermo Fisher Scientific, Waltham, MA, USA) were used to make evaluation reproducible by analyzing the volume containing 5000 beads for each sample. EVs were analyzed with LSR Fortessa X-20 Cell Analyzer (BD Biosciences, San Jose, CA), and data were calculated using the FACS DIVA 8.0 software (BD Biosciences).

miRNA analysis of EVs

RNA was extracted from 100 μL of EVs isolated from eight OP, nine OPN, and eight CN subjects. Two-hundred nanograms of RNA isolated with ExoRNeasy Serum/Plasma kit (QIAGEN, Hilden, Germany) were sent to QIAGEN Genomic Services and used to perform the analysis of miRNome-wide quantification of mature

miRNA by next-generation sequencing (NGS). miRNA analysis was performed according to Rossi et al.[16] Briefly, after assessing the purity of vesicle RNA by a NanoDrop 2000 spectrophotometer (Thermo Fisher Scientific), the complete miRNome was evaluated using a QIAseq miRNA Library kit (QIAGEN, Hilden, Germany) after sequencing by Illumina-based NextSeq 500 technology. Data were mapped to miRbase_20 database, and thereafter the number of known miRNAs was calculated. Sequencing of EV-miRNAs generated an average of 1.07 million reads per sample, and the average genome-mapping rate was 11.6%. A miRNA with a log2-fold change log2N ≥ 1.5 was considered upregulated, while log2N ≤ −1.5 was identified as a downregulated miRNA. Moreover, to explore the regulatory function of miRNAs, gene ontology (GO) analysis was performed with the R package TopGO with experimentally verified targets of significantly differentially expressed miRNAs as input.

miRNA validation by real-time PCR

Validation of altered miRNAs was performed on RNA extracted from EVs of six OP, six OPN, and seven CN subjects. From 10 ng total RNA, miRNAs were reverse transcribed using TaqMan Advanced miRNA cDNA synthesis kit (Thermo Fisher Scientific) according to the manufacturer's instructions. TaqMan microRNA assay was performed using QuantStudio 7 Pro Real-Time PCR System (Thermo Fisher Scientific). The miRNA sequences and assay numbers are listed in Table S1.

Proteomic analysis

The vesicles derived from plasma samples were resuspended in PBS and then in an equal volume of 2,2,2-trifluoroethanol. The samples were vortexed and sonicated for 6 minutes in an ice bath and finally incubated with constant shaking at 60°C for 2 hours. Proteins were quantified by Bicinchoninic Acid (BCA) assay (Thermo Fisher Scientific), and 100 μg were digested with trypsin according to Duijvesz et al.[17] After 18 hours of digestion at 37°C with constant shaking, the reaction was stopped adding 50 μL of 2.5% trifluoroacetic acid (TFA) was ad. Samples were then centrifuged at 14,000*g* for 10 minutes at 4°C, desalted, and concentrated using 100 μL OMIX C18 pipette tips (Agilent Technologies, Santa Clara, CA, USA), dried by speed vacuum, and finally resuspended in aqueous solution containing 5% acetonitrile (ACN) and 0.1% formic acid (FA). Tryptic peptides were subjected to nano-high-resolution liquid chromatography-electrospray ionization-tandem mass spectrometry (nano-HPLC-ESI-MS/MS) analysis performed on an Eksigent Ekspert Nano LC400 system (Sciex, Toronto, ON, Canada) and directly coupled to a TripleTOF 5600$^+$ (Sciex) with a nanoESI source (NANOSpray III, Sciex). Two micrograms of tryptic digests from each sample were injected and preconcentrated for 5 minutes on an Acclaim PepMap 100 C18 trap column (5 μm particle size, 100 Å pore size, 100 μm i.d. × 2 cm, ThermoFisher Scientific), at a flow rate of 3 μL/minute using solvent A (aqueous solution of 2% ACN and 0.1% FA) as mobile phase, and then separated by reverse-phase chromatography performed on an Acclaim PepMap100 C18 column (3 μm particle size, 100 Å pore size, 75 μm i.d. × 25 cm, ThermoFisher Scientific) at a flow rate of 300 nL/min and temperature of 40°C, by a two-step gradient of solvent B (ACN/water 98:2, v/v, final 0.1% FA) from 5% to 25% in 120 minutes. Mass spectra were collected by the mass spectrometer operating in positive ion mode and in information-dependent acquisition (IDA) scan mode in which each full mass spectrometric scan (mass range: 350–1250 m/z, acquired in 0.25 second) was followed by data-dependent fragmentation experiments (MS/MS) of the 35 most abundant multiple-charged precursor ions via collision-induced dissociation (CID) with accumulation time set to 0.1 second from 230–1500 m/z. To avoid redundant sequencing of the most abundant peptides, the active exclusion was enabled for 15 seconds. Three technical replicates for each biological replicate were acquired. The data analysis, statistical methods, and Weighted Gene Co-Expression Network Analysis (WGCNA) are described in the supplementary materials.

Bone cell treatment with EVs

The isolation and culture of bone cells are described in the supplementary materials. One million/cm^2 of healthy donor (HD) peripheral blood mononuclear cells (PBMCs) were seeded in a 96-well culture plate. After 3 hours, nonadherent cells were removed and cultures were maintained under four different conditions: (i) medium with 1% FBS ultracentrifuged to remove serum EVs + 20 ng/mL M-CSF + 30 ng/mL RANKL, (ii) medium with 1% ultracentrifuged FBS + 2 μg/μL of CN EVs (90 μL), (iii) medium with 1% ultracentrifuged FBS + 2 μg/μL of OPN EVs (90 μL), and (iv) medium with 1% ultracentrifuged FBS + 2 μg/μL of OP EVs (90 μL). The medium was changed every 3–4 days; after 2 weeks, cells were fixed in 4% formaldehyde and stained with histochemical staining of TRAcP (Sigma-Aldrich, St. Louis, MO, USA; Catalog No. 387) to evaluate the number of mature osteoclasts.

To evaluate gene expression, mature osteoclasts and osteoblasts were treated with 2 μg/μL (90 μL) of EVs from CN, OPN, or OP patients in the absence of serum. After 48 hours, RNA was extracted, 1 μg was reverse transcribed (SensiFAST cDNA synthesis kit, Bioline, UK) in a volume of 20 μL to produce complementary DNA (cDNA), and 25 ng of cDNA was used for Real-Time RT-PCR reactions using SensiFAST SYBR Low-ROX kit (Bioline, London, UK). The fold change in gene expression was calculated with the delta-delta-cycle threshold (DDCT) method.[18] Primer sequences for gene expression analysis of osteoclast and osteoblast cultures are listed in Table S2.

For the evaluation of bone resorption, control PBMCs were cultured on bovine bone slices for 2 weeks in the presence of M-CSF/RANKL and then treated with a pool of EVs from CN, OPN, or OP subjects for 4 days. Bone slices were cleaned free of cells by sonication; then they were stained with 1% toluidine blue and observed by conventional light microscopy. Resorption area was measured by image analysis system (NIS Elements BR 4.50.00).

The osteogenic differentiation ability of MSCs was evaluated by incubating cells with αMEM, 10% EVs-depleted FBS, 50 U/mL penicillin, 50 mg/mL streptomycin, and 2 mM L-glutamine supplemented with 10^{-7} M dexamethasone, 50 μg/mL L-ascorbic acid, 5 mM β-glycerophosphate, and 2 μg/μL (90 μL) pool of EVs from CN, OPN, and OP patients. The osteoblastogenic medium and EVs were changed every 3 days; after 2 weeks of culture, cells were fixed with 4% formaldehyde in PBS and stained for ALP.

Bone cell treatment with miR-1246 mimic

Osteoclast precursors were derived from PBMCs of HDs cultured for 10 days with 20 ng/mL M-CSF and 30 ng/mL RANKL. Then

the cells were treated with 500 nM miR-1246 mimic (Thermo Fisher Scientific) and negative control (Thermo Fisher Scientific). After 4 days, cells were fixed in paraformaldehyde and stained for TRAcP to count osteoclasts, or RNA expression analysis was performed.

Osteoblasts isolated from bone fragments of healthy subjects (see supplementary materials) were treated with 200 nM miR-1246 mimic or with negative control for 48 hours, then RNA was extracted as previously described.

Statistical analysis

Data from different experimental conditions are expressed as boxplots with median. Data were tested for normality by Kolmogorov–Smirnov. Values were then compared by unpaired *t*-test if data pass normality tests or by nonparametric Mann–Whitney U test, when appropriate. All *p*-values are two-sided and considered significant for $p \leq 0.05$. Analyses were performed through GraphPad Prism 8.

Results

Patient descriptions

In the OP group, 10 patients had a morphometric vertebral fracture, and 2 had a wrist fracture. We found no difference in anthropometric parameters between OP, OPN, and CN (Table 1).

Biochemical evaluation revealed no statistically significant differences between the three groups of subjects as regards serum calcium, creatinine, phosphate, PTH, 25 (OH) D, BALP, RANKL, OPG and RANKL/OPG ratio and interleukin (IL)-6 (Table 1). CTX levels were increased in the OP group compared to the CN subjects.

EV characterization

To evaluate the role of EVs in OP patients, we first characterized EVs isolated from plasma. The vesicular nature of the particles obtained by ultracentrifugation was assessed by TEM, which demonstrated the presence of heterogeneous population of vesicles with spherical shape distributed as single entities or grouped in small clusters (Fig. 1*A*). In all the experimental groups, the diameter of EVs ranges from 30 to 500 nm; the isolated EVs were mainly smaller than 200 nm, suggesting an enrichment of exosome population (Fig. 1*A*). Vesicles with diameters of 400–500 nm were rare.

To confirm the membrane integrity of EVs and to discriminate EVs from background noise, we performed FACS analysis after incubation with CFSE dye. FACS analysis revealed that OP patients present a significantly increased number of vesicles compared to both CN and OPN subjects (Fig. 1*B,C*). Interestingly, EV protein content was increased in OP and OPN groups compared to CN subjects, whereas no significant alterations were detected between EV samples from OP and OPN patients (Fig. 1*D*). Moreover, we evaluated the presence of membrane-bound RANKL in EVs observing a significant increase in the number of $RANKL^+$ EVs in OP compared both to CN and OPN subjects (Fig. 1*E,F*).

Total EVs were negatively associated with the T-score at the lumbar spine (beta $= -0.45$, $p < 0.05$) and femoral neck (beta $= -0.48$, $p < 0.05$). An inverse correlation was observed between $RANKL^+$ EVs and T-score at the lumbar spine (beta $= -0.49$, $p < 0.05$) and femoral neck (beta $= -0.54$, $p < 0.05$). We found no association between bone turnover markers (CTX and BALP) and T-scores or EVs and BTM (data not shown). Only in the OPN patients there was a direct correlation between the total number of vesicles and the serum RANKL (beta $= 0.70$, $p = 0.009$); similarly, the $RANKL^+$ EVs were positively associated with the serum RANKL (beta $= 0.64$, $p = 0.03$).

miRNome analysis of EV

Because EVs act as cell–cell communication vectors and are able to transfer miRNAs, we performed miRNome analysis to characterize miRNA content in our experimental groups. Results from NGS analysis reported 63 miRNAs robustly expressed (>100 reads) in EV samples from CN and OP/OPN patients (Fig. 2*A*). Fourty-nine miRNAs were commonly expressed in all the groups, whereas miR-144-3p and miR-454-3p were present exclusively in

Table 1. Mean ± SD Values of Main Anthropometric, Biochemical, and Densitometric Parameters of the Three Groups of Subjects Divided According to T-Scores

	CN	OPN	OP
Age (years)	61.9 ± 6.8	62.2 ± 7.9	64.5 ± 9.8
BMI (kg/m^2)	25.4 ± 3.2	25.7 ± 2.3	24.7 ± 3.7
Femural neck T-score	−0.43 ± 0.35	−1.27 ± 0.78	−2.9 ± 0.80[a,b]
L1-L4 T-score	−0.35 ± 0.48	−1.12 ± 0.64	−2.28 ± 0.77[a,b]
Calcium (mg/dL)	9.3 ± 0.5	9.3 ± 0.4	9.4 ± 0.4
Creatinine (mg/dL)	0.81 ± 0.18	0.78 ± 0.11	0.74 ± 0.11
Phosphate (mg/dL)	3.5 ± 0.4	3.8 ± 0.5	3.6 ± 0.5
PTH (pg/mL)	25.0 ± 7.7	26.2 ± 13.4	24.4 ± 11.4
25(OH)D (ng/mL)	26.7 ± 9.4	25.7 ± 10.0	26.6 ± 11.8
BALP (U/L)	14.8 ± 7.0	14.7 ± 6.5	10.8 ± 4.9
CTX (ng/mL)	0.40 ± 0.15	0.49 ± 0.20	0.51 ± 0.13[b]
RANKL (pmol/L)	202.14 ± 94.47	246.6 ± 216.6	222.4 ± 133.3
OPG (pmol/L)	10.0 ± 3.5	8.5 ± 3.2	9.0 ± 2.9
RANKL/OPG	26.1 ± 27.7	32.3 ± 26.9	28.1 ± 20.0
IL-6 (pg/mL)	2.32 ± 2.2	2.2 ± 0.3	2.0 ± 0.4

CN: Controls (T-score > −1.0 SD); OPN: Osteopenic (−1.0 > T-score > −2.5 SD); OP: Osteoporotic (T-score < −2.5 SD).
[a] $p < 0.05$ OP vs OPN.
[b] $p < 0.05$ OP vs CN.

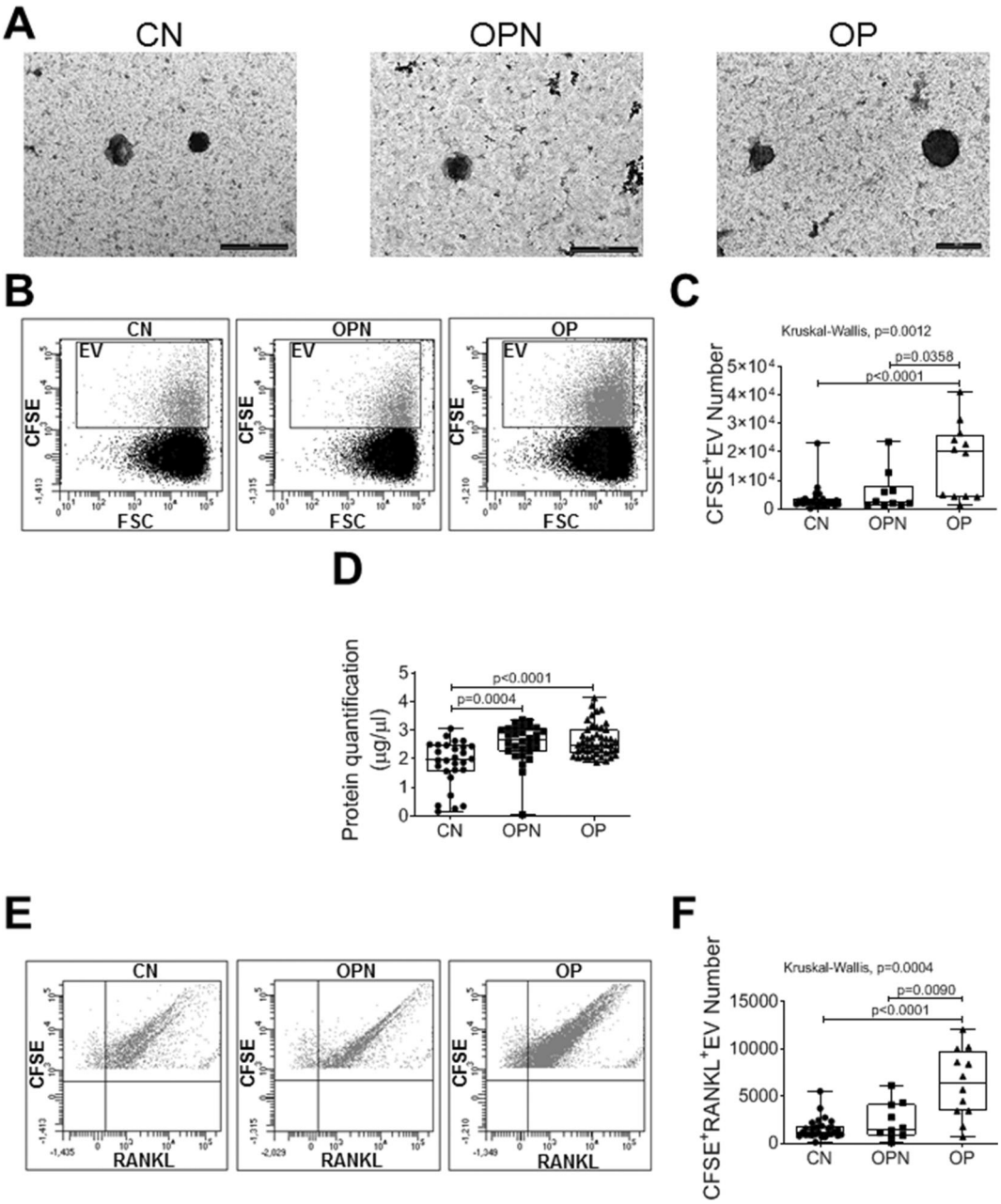

Fig. 1. Extracellular vesicle (EV) characterization. (*A*) Transmission electron microscopy analysis of EVs from controls (CN), osteopenic (OPN) and osteoporotic (OP) patients. (*B*) Dot-plot of EVs isolated from CN, OPN, and OP women isolated by ultracentrifugation. Extracellular vesicles were loaded with CFSE and analyzed by FACS. (*C*) Quantification of EV number in 28 controls, 10 OPN and 12 OP samples. (*D*) Protein amounts in EV samples from different groups (28 CN, 30 OPN and 47 OP subjects). (*E*) Dot-plot of 28 CN, 10 OPN and 12 OP EVs loaded with CFSE and labeled with RANKL antibody. (*F*) Absolute quantification of $RANKL^{+}$ EVs. Boxplots with individual data points and exact *p*-values are shown.

OP samples (Fig. 2*A*). miR-186-5p, miR-146b-5p and miR-374a-5p were specific for OPN subject–derived EVs, while miRNA-99-5p was exclusive for CN EVs (Fig. 2*A*).

In EV samples isolated from OP patients, significant modulation of 12 miRNAs (Fig. 2*B*, Table S3) was observed compared to CN EVs; indeed, 7 miRNAs were upregulated and 5 downregulated (Table S3). The most upregulated miRNA was miR-1246.

Differentially expressed miRNAs are involved in 66 biological processes, including the regulation of vitamin D receptor signaling (GO:0070562), osteoclast differentiation (GO:0030316), trabecular formation (GO:0060343), and IL-13 production (GO:0032616) pathways (Table S4).

In the comparison of OP EVs and OPN EVs, the miRNA large-array analysis revealed 6 upregulated and 9 downregulated miRNAs (Fig. 2*C*, Table S5), involved in the regulation of 192 biological processes (Table S6), including the transforming growth factor beta signaling (GO:0071636; GO:0007179), biomineral tissue development (GO:0031214, GO:0030501, GO:0070169), osteoblast differentiation/activity

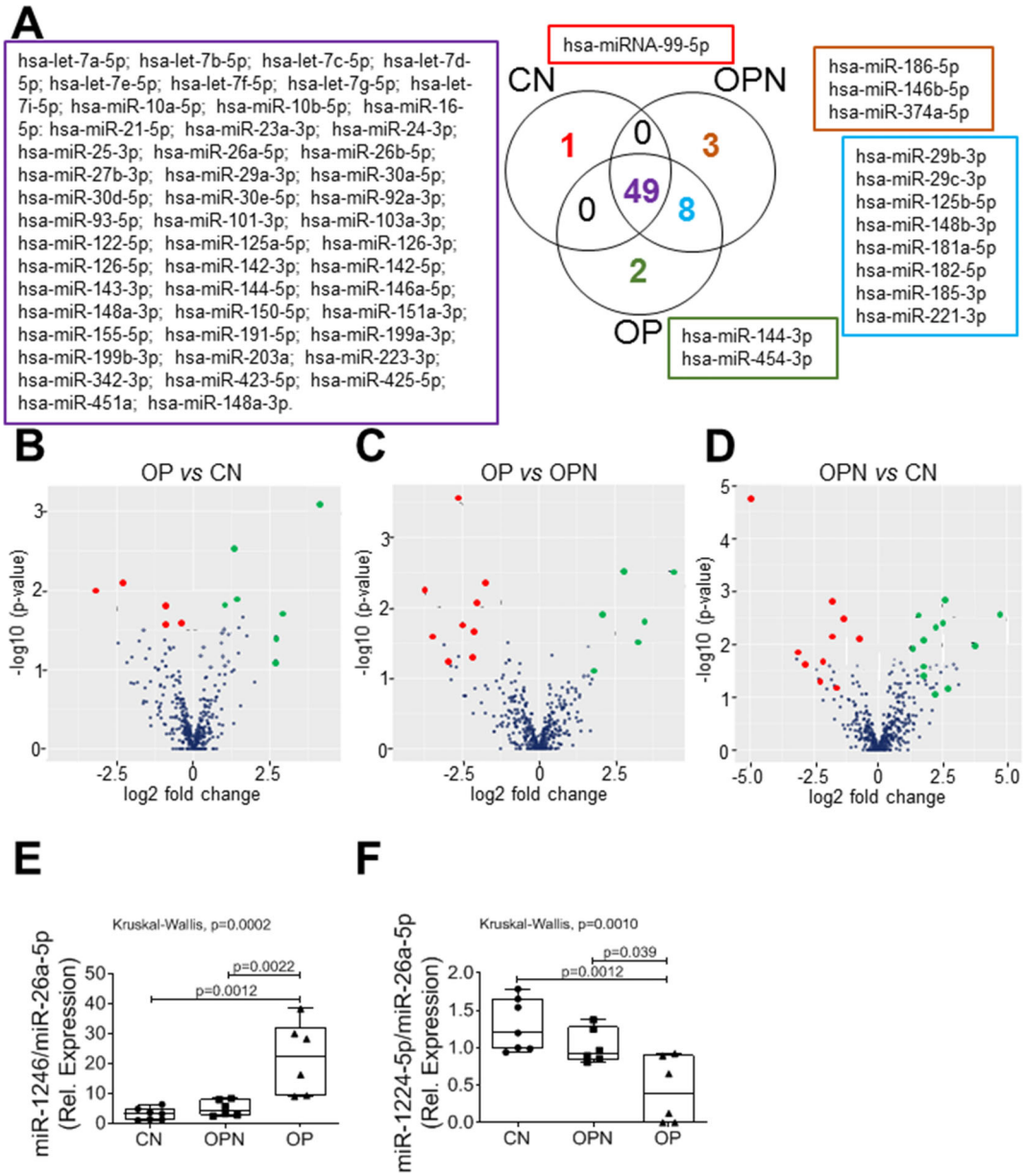

Fig. 2. miRNome analysis of extracellular vesicles (EVs). (*A*) Venn diagram comparing miRNAs detected in EVs from eight controls (CN), nine osteopenic (OPN) and eight osteoporotic (OP) patients. MiRNAs for each group are listed in the colored box (purple: shared miRNAs between CN, OPN and OP; red: exclusive for CN; orange: exclusive for OPN; green: exclusive for OP; light blue: shared between OPN and OP). (*B–D*) Volcano plot of differentially expressed human mature miRNAs in (*B*) OP vs CN, (*C*) OP vs OPN, and (*D*) OPN vs CN. *p*-value (−log10) is plotted on *y*-axis and the expression fold change between the two experimental groups on the *x*-axis. Statistically significant upregulated and downregulated miRNAs are marked in green and red, respectively. (*E, F*) Validation by Real-Time RT-PCR expression analysis of (*E*) miR-1246 and (*F*) miR-1224-5p in EVs from seven CN, six OPN and six OP subjects. Boxplots with individual data points and exact *p*-values are shown.

(GO:0045669), and regulation of osteoclast differentiation (GO:0045670).

The same analysis was performed between EVs from OPN and controls; we identified 12 upregulated and 10 downregulated miRNAs in EVs from OPN subjects compared to CNs (Fig. 2*D*, Table S7). Gene ontology analysis revealed a modulation of 132 pathways, including those involved in trabecular formation (GO:0060343), biomineral tissue development (GO:0031214), and vitamin D receptor signaling (GO:0070562) (Table S8).

The levels of the most upregulated miR-1246 and the most downregulated miR-1224-5p in OP EVs were further confirmed by Real-Time RT-PCR expression analysis (Fig. 2*E,F*).

Proteomic analysis of circulating EVs

The protein profile of EVs was subjected to nano-liquid chromatography tandem mass spectrometry (nLC–MS/MS) analysis. A total of 376 proteins were identified and quantified in all EV samples, but after filtering for the presence of at least 2 peptides for

each protein, 240 final proteins were taken into consideration. In particular, 210 proteins were identified in CN EVs, 180 in OPN EVs, and 195 in OP EVs (Fig. 3*A*).

A Venn diagram showed 147 shared proteins among the 3 groups. The comparison highlighted 17 specific proteins in CN EVs, 10 in OPN EVs, and 15 in OP EVs (Fig. 3*A*).

Bioinformatic analysis was then performed in order to identify the main biological pathways associated with the differentially expressed proteins. PANTHER analysis revealed the four most represented biological processes, including blood coagulation, gonadropin-releasing hormone receptor, inflammation mediated by chemokine and cytokine signaling, and plasminogen activade cascade pathways (Fig. 3*B*).

Univariate analysis highlighted several differentially expressed proteins in each comparison between group conditions: 38 proteins were differentially expressed in OPN EVs versus CN EVs, 49 in OP EVs versus CN EVs, and 53 in OP EVs versus OPN EVs (Table S9). The comparison between OPN and CN EVs evidenced a slight decrease in fibrinogen and clusterin and an increase in apolipoprotein (Table S10). In OPN EVs, the analysis revealed reduced

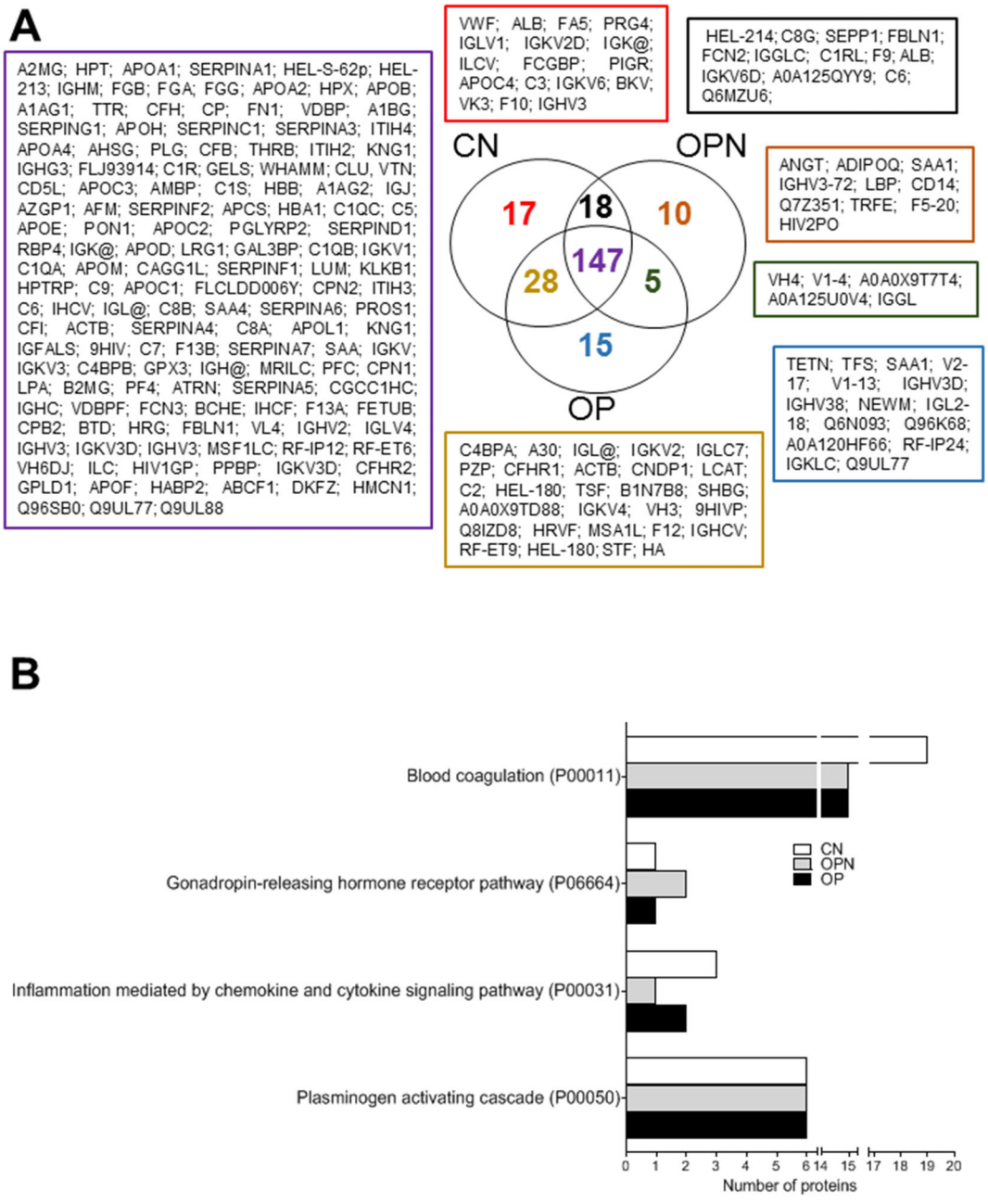

Fig. 3. (*A*) Venn diagram showing number of identified proteins and their distribution in the three extracellular vesicles (EVs) groups [nine controls (CN), nine osteopenic (OPN), and nine osteoporotic (OP) patients. Proteins for each group are listed in the colored box (purple: shared protein expressed in CN, OPN and OP; red: exclusive for CN; orange: exclusive for OPN; light blue: exclusive for OP; yellow: shared between OP and CN; black: shared between CN and OPN; green: shared between OPN and OP). (*B*) Graphical representation of most represented biological processes and number of proteins involved in EV groups derived from PANTHER analysis.

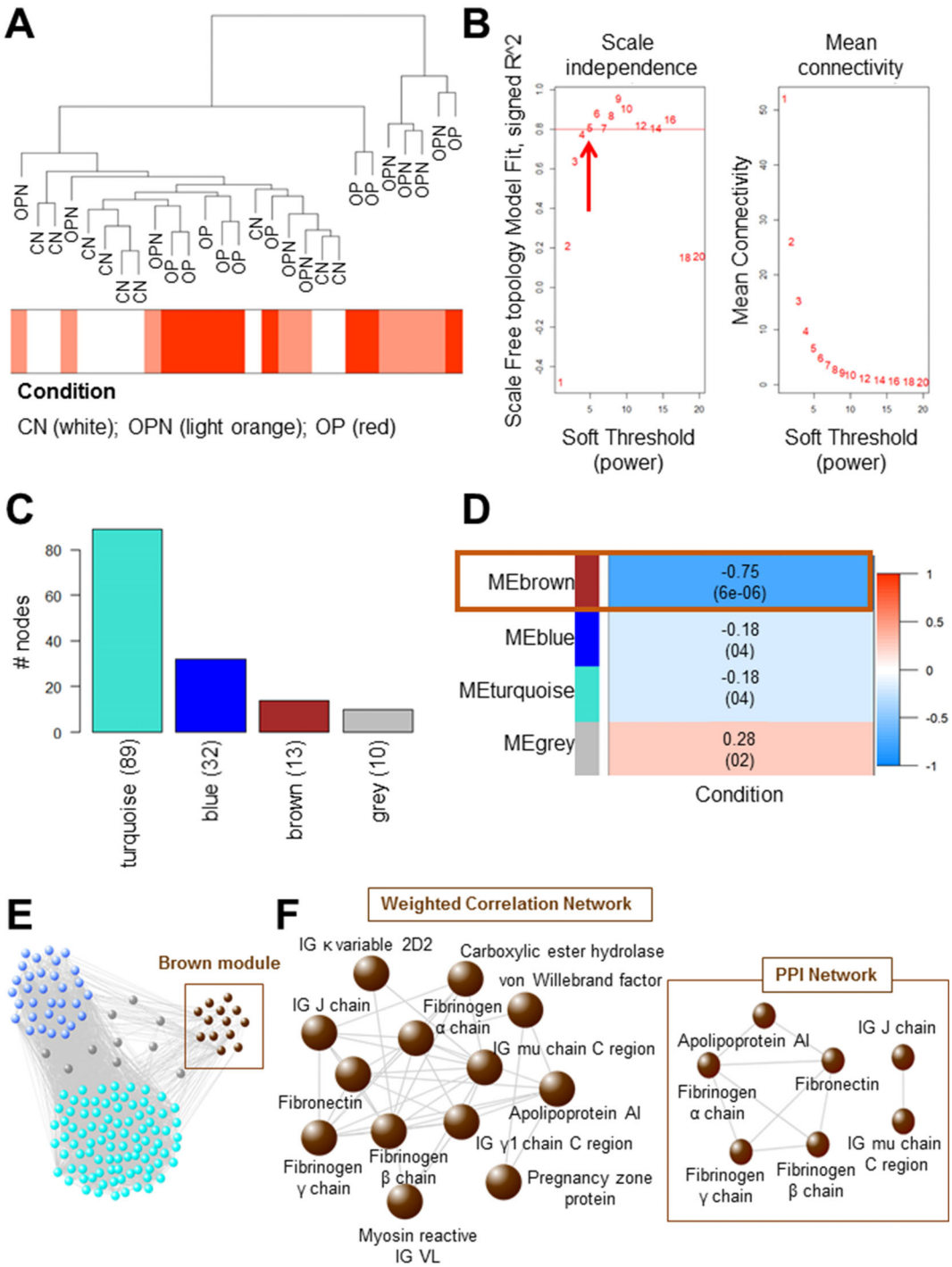

Fig. 4. Weighted gene co-expression network analysis (WGCNA). (*A*) Clustering dendrogram of samples. Sample clustering was conducted to detect outliers. The Euclidean distance correlation was used as distance metrics. All samples are located in the clusters and passed the cutoff thresholds. The horizontal bars represent how the osteoporotic (OP)/osteopenic (OPN)/control (CN) conditions relate to the sample dendrogram: White (low value) represents control samples, light red (median value) represents OPN samples, and red (high value) represents OP samples. (*B*) Calculation and selection of optimal soft-thresholding power. Influence of different powers on scale independence (*left panel*) and on mean connectivity (*right panel*). The selected soft-thresholding power is indicated by a red arrow. (*C*) WGCNA module barplot. The bars show the size of each WGCNA detected module and the color represents the corresponding module labels. (*D*) Module-trait associations. In a heatmap, each row corresponds to a module eigengene, and each cell contains the corresponding correlation and *p*-value with OP/OPN/CN condition. The table is color-coded by correlation according to the color legend on the right. (*E*) WGCNA network. The highlighted brown module represents a unique statistically significant module, associated with the OP/OPN/CN condition. In the WGCNA correlation network, the color of nodes is associated with the detected modules according to the labels. (*F*) WGCNA network. Correlation-based interactions among proteins belonging to brown module in the WGCNA network (*left panel*). Protein–protein interaction network. Physical interactions among proteins of brown module in human interactome (*right panel*).

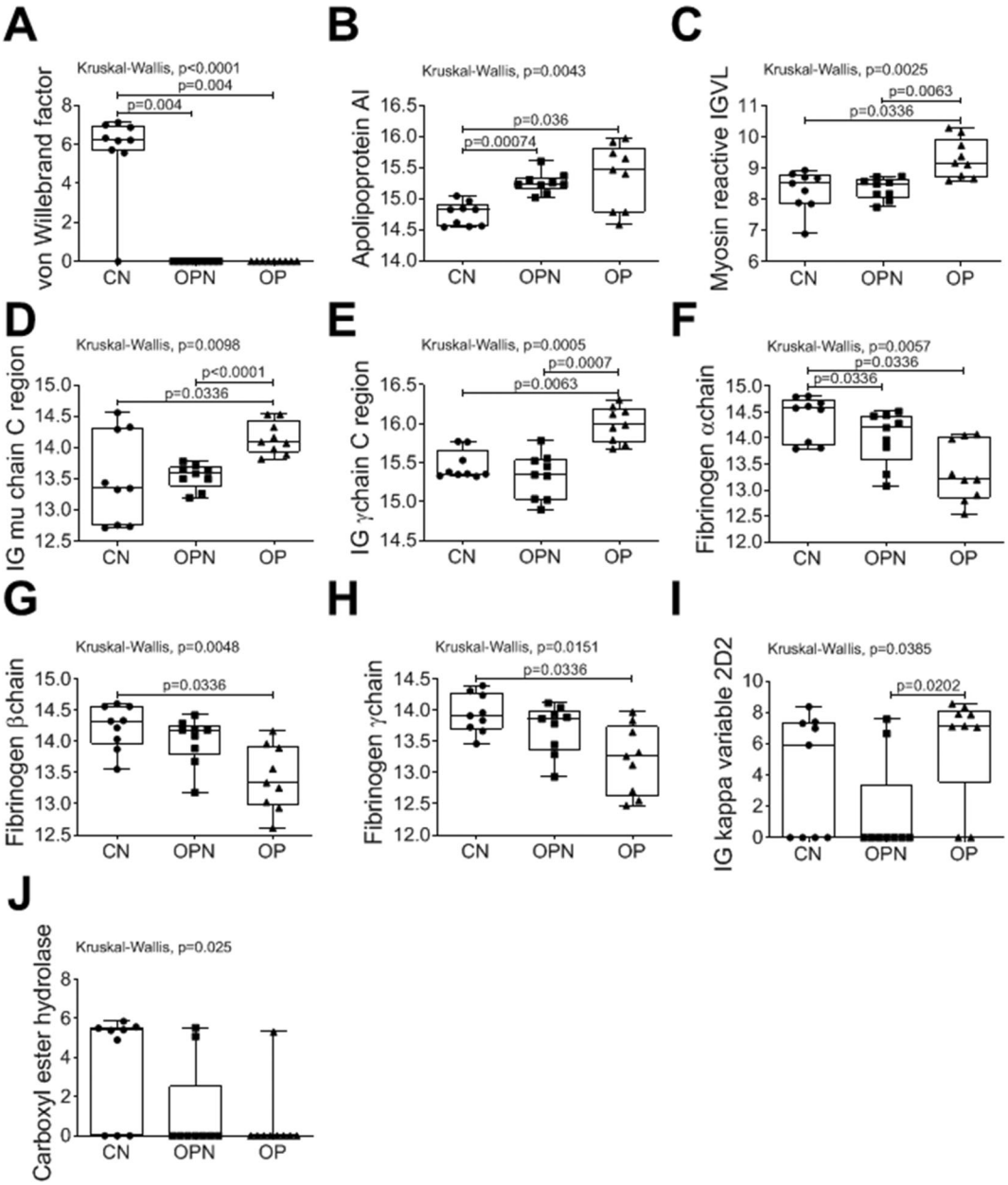

Fig. 5. Detailed graphs of the 10 statistically significant proteins of the brown module in extracellular vesicles (EVs) from nine controls (CN), nine osteopenic (OPN), and nine osteoporotic (OP) patients. (*A*) von Willebrand factor, (*B*) apolipoprotein AI, (*C*) myosin reactive immunoglobulin light chain variable region (IGVL), (*D*) immunoglobulin (IG) mu chain C region, (*E*) IG γ chain C region, (*F*) fibrinogen α chain, (*G*) fibrinogen β chain, (*H*) fibrinogen γ chain, (*I*) IG kappa variable 2D2, (*J*) carboxyl ester hydrolase protein expression in CN, OPN and OP EVs. Boxplots with individual data points and exact *p*-values are shown.

vitronectin and increased coagulation factor expression compared to CN EVs (Table S10). Moreover, the modulation of apolipoproteins was also observed in a comparison of OP EVs and CN EVs (Table S10).

WGCNA network analysis

WGCNA was performed to identify a similar profile of protein modules in the sample population considering the trait of interest (condition). Sample clustering was conducted to detect outliers and visualize how the condition (i.e., OP/OPN/CN status) was associated with the sample grouping (Fig. 4*A*). The clustering algorithm identified two main clusters and the samples according to condition (Fig. 4*A*).

The weighted network was built using a Pearson's correlation matrix and a soft thresholding power equal to 5 (Fig. 4*B*). The final network consisted of 4 modules (labeled by color), ranging in size from 10 to 89 members (Fig. 4*C*). The gray module showed the grouping of nodes with outlying profiles and was not further considered. Only the brown module ended up being statistically

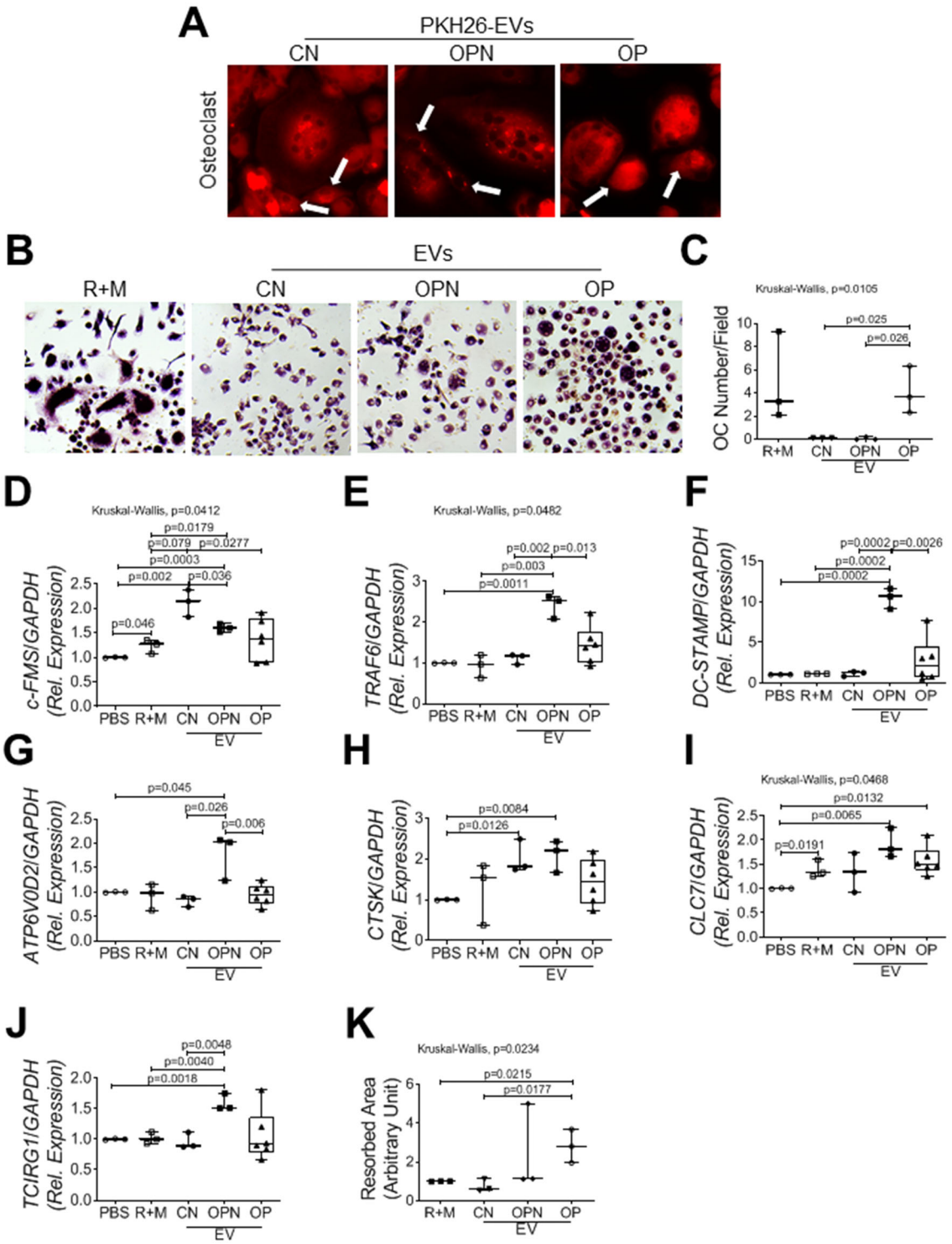

Fig. 6. Effect of extracellular vesicles (EVs) on healthy donor (HD) osteoclasts. (*A*) PKH26 EVs are able to fuse with HD osteoclasts and osteoclast precursors (white arrows). Original magnification: ×20. (*B, C*) HD peripheral blood mononuclear cells were treated for 2 weeks with (i) medium with 1% ultracentrifuged FBS +- 20 ng/mL M-CSF + 30 ng/mL RANKL, (ii) medium with 1% ultracentrifuged FBS + control (CN) EVs, (iii) medium with 1% ultracentrifuged FBS + osteopenic (OPN) EVs, (iv) medium with 1% ultracentrifuged FBS + osteoporotic (OP) EVs. For treatment an EV pool from 10 CN, 10 OPN, and 10 OP subjects was used. (*B*) Representative pictures of TRAcP staining. Original magnification ×20. (*C*) Number of TRAcP positive multinucleated (>3 nuclei) cells. (*D–J*) HD osteoclasts were treated with pool of EVs from 10 CN, 10 OPN, or 10 OP patients, and after 48 hours RNA was extracted. Real-time RT-PCR expression analysis was performed for (*D*) *c-FMS*, (*E*) *TRAF6*, (*F*) *DC-STAMP*, (*G*) *ATP6V0D2*, (*H*) *CTSK*, (*I*) *CLC7*, and (*J*) *TCIRG1* genes. (*K*) Bone resorption analysis of three HD osteoclasts plated on bovine bone slices and treated with an EV pool of 10 CN, 10 OPN, and 10 OP patients. Boxplots with individual data points and exact *p*-values are shown.

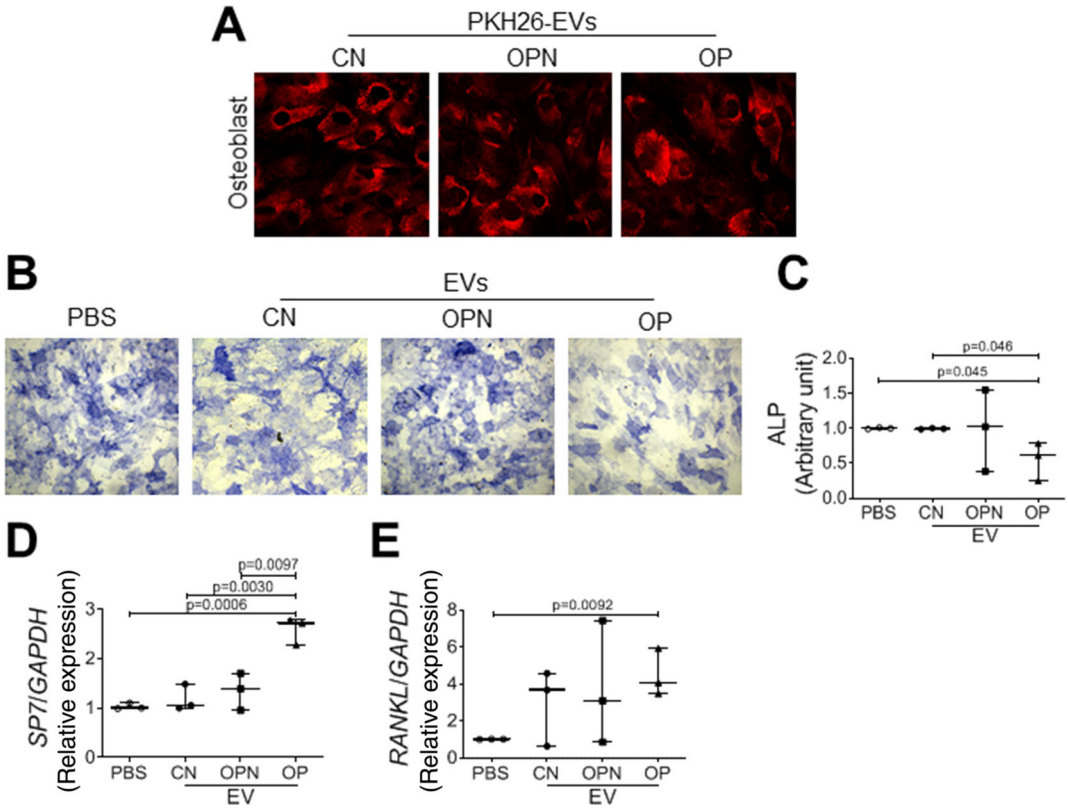

Fig. 7. Effect of extracellular vesicles (EVs) on healthy donor (HD) osteoblasts. (*A*) PKH26 EVs from control (CN), osteopenic (OPN), and osteoporotic (OP) subjects are able to fuse with HD osteoblasts. Original magnification: ×20. (*B*, *C*) Mesenchymal stem cells (MSCs) from three HDs were differentiated with osteogenic medium and 10 CN, 10 OPN, and 10 OP EV pools. (*B*) Alkaline phosphatase staining (original magnification ×10) and (*C*) densitometric analysis. (*D*, *E*) Real-time RT-PCR expression analysis of RNA extracted from three HD osteoblasts treated for 48 hours with pool of EVs from 10 CN, 10 OPN, and 10 OP patients. Gene expression analysis of (*D*) *SP7* and (*E*) *RANKL*. Boxplots with individual data points and *p*-values are shown.

significant (*p*-value 6×10^{-6}). The values for module membership (MM), biomarker significance (BS), and the associated *p*-values were reported for the brown module in Table S11. Moreover, in Fig. 4*D* was reported the result of association testing among OP/OPN/CN conditions. In particular, the brown module highlighted high negative correlations (i.e., −0.75) with the condition, meaning that the proteins falling in this module were mainly expressed in controls with respect to patients (OP/OPN) (Fig. 4*D*).

To better discriminate the statistically significant differential proteins in the brown module associated with condition, the network was exploded (Fig. 4*E*). In particular, this module included a total of 13 proteins with similar patterns that could be closely coregulated, functionally related, or members of the same pathway. These proteins were classified according to their BS and are reported in Fig. 4*F* and Table S11. A positive sign of the BS value means that the protein is mainly expressed in patients (OP/OPN), whereas a negative sign indicates that the protein increases in the CN group (Table S11).

Finally, proteins belonging to the brown module, identified in the WGCNA, were mapped on the human interactome [protein–protein interaction (PPI) network][19] in order to identify the molecular interconnections (Fig. 4*F*) in which the von Willebrand factor showed the highest correlation value within module degree and the highest BS coefficient.

Moreover, a detail of the 10 statistically significant comparisons for OP/OPN/CN are reported in Fig. 5. The comparison highlighted that von Willebrand factor is completely absent in EVs from patients with low bone mass (Fig. 5*A*). EVs from patients with low BMD are rich in apolipoprotein AI (Fig. 5*B*), myosin-reactive immunoglobulin light chain variable region (IGVL) (Fig. 5*C*) and immunoglobulin (IG) chains (Fig. 5*D*,*E*) and are characterized by reduced fibrinogen chains (Fig. 5*F*–*H*); modulation of IG kappa variable 2D2 and carboxyl ester hydrolase was also observed (Fig. 5*I*,*J*).

EVs' effect on bone cells

EV characterization prompted us to investigate the role of EVs in the etiopathogenesis of osteoporosis. Because of the higher number of RANKL-positive EVs in OP, we evaluated their possible role in osteoclast formation. To assess the ability of EVs to fuse with bone cells, we incubated osteoclasts with PKH26-labeled EVs. Microscopic analysis revealed that EVs from OP and OPN subjects integrated into osteoclasts and osteoclast precursors (Fig. 6*A*) as well as those from controls.

We treated HD PBMCs with the same number of EVs for each experimental group; interestingly, EVs from OP subjects were able to induce osteoclastogenesis at the same level observed following RANKL and M-CSF treatment. CN and OPN EVs were not able to support the differentiation of PBMC into osteoclasts (Fig. 6*B*,*C*). Moreover, to evaluate the effects of the treatment on osteoclast markers, we treated mature HD osteoclasts for

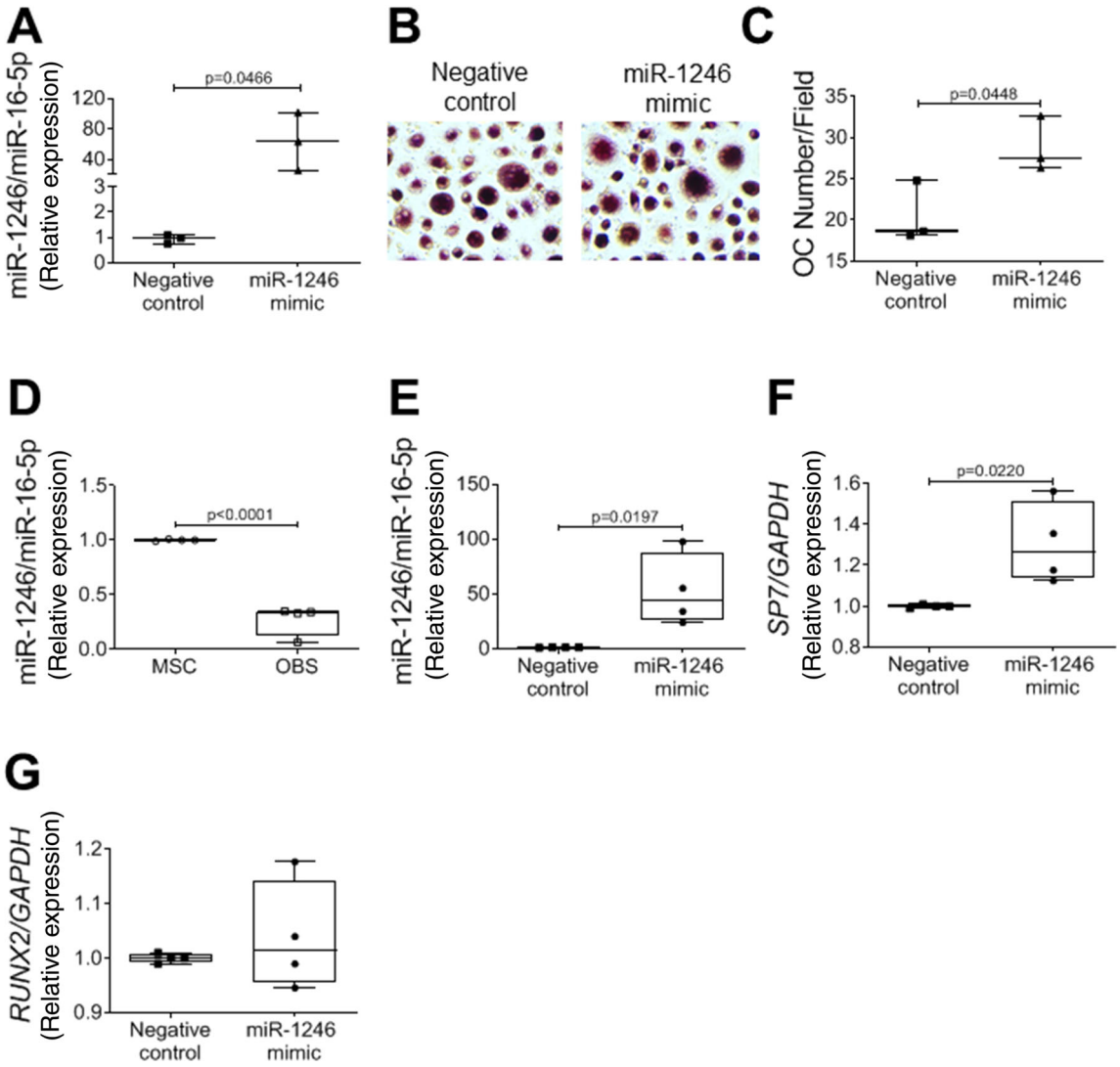

Fig. 8. MiR-1246 upregulation in bone cells. (*A–C*) Three healthy donor (HD) peripheral blood mononuclear cells were treated for 10 days with M-CSF/RANKL to obtain osteoclast precursors and then with (i) medium with 10% FBS + 20 ng/mL M-CSF + 30 ng/mL RANKL +500 nM negative control of miRNA mimic, (ii) medium with 10% FBS + 20 ng/mL M-CSF + 30 ng/mL RANKL +500 nM miR-1246 mimic for 4 days. (*A*) Real-time RT-PCR expression analysis of miR-1246. (*B*) Representative pictures of TRAcP staining. Original magnification ×20. (*C*) Number of TRAcP positive multinucleated (>3 nuclei) cells. (*D*) Real-time RT-PCR expression analysis of miR-1246 during osteoblast differentiation. RNA was isolated from four HD mesenchymal stem cell (MSC) and osteoblast (OBS) cultures; OBSs were obtained after 21 weeks of MSC differentiation with osteogenic medium. (*E–G*) Real-time RT-PCR expression analysis of four HD OBS treated for 48 hours with (i) medium with 10% FBS + lipofectamine +200 nM negative control of miRNA mimic and (ii) medium with 10% FBS + lipofectamine +200 nM miR-1246 mimic. Expression analysis of (*E*) miR-1246, (*F*) *SP7*, and (*G*) *RUNX2*.

48 hours with EVs. Surprisingly, Real-Time RT-PCR expression analysis showed that OPN EVs could support osteoclast differentiation and function, suggesting an important role of EVs in the progression of osteoporosis. In fact, there was an increase in *c-FMS* (Fig. 6*D*), *TRAF6* (Fig. 6*E*), *DC-STAMP* (Fig. 6*F*), *ATP6V0D2* (Fig. 6*G*), *CTSK* (Fig. 6*H*), *CLC7* (Fig. 6*I*), and *TCIRG1* (Fig. 6*J*) genes when osteoclasts were treated with OPN EVs. Moreover, OP EVs stimulated the bone resorption ability of HD osteoclasts plated on bovine bone slices (Fig. 6*K*).

For completeness, we evaluated the effect of EVs on osteoblast formation. EVs PKH26-labeled from OP and OPN patients combined with osteoblasts as well as those from the CN (Fig. 7*A*). HD MSCs were differentiated in the presence of osteogenic medium and EV pools. OP EVs reduced the ability of MSCs to differentiate into osteoblasts, as revealed by ALP staining (Fig. 7*B*,*C*).

On the other hand, on mature osteoblasts, OP EVs induced an increase of *SP7* (Fig. 7*D*) and *RANKL* (Fig. 7*E*) genes, whereas no significant alterations were observed for *COL1A2*, *ALP*, *RUNX2*, *OPG*, and RANKL/OPG Ratio (Fig. SS1*A–E*).

EVs in patients with GSD

To investigate whether alterations of circulating EVs could also be observed in patients with other bone loss disease, we isolated EVs from seven patients affected by GSD and revealed an increase in $RANKL^+$ EVs [$RANKL^+$ EV/Total EV (%); HD EVs:

19.53 ± 5.83; GSD EVs 31.79 ± 17.25; $p < 0.042$]. Upregulation of exosomal miR-1246 was revealed in samples of 10 GSD patients (Relative expression. HDs: 0.99 ± 0.66; GSD patients: 3.45 ± 2.92, $p < 0.028$).

MiR-1246 in bone cells

Since we previously demonstrated that miR-1246 is upregulated during osteoclastogenesis, we evaluated the effects of miR-1246 mimic treatment on the capacity for osteoclastogenesis of HD osteoclast precursors. First, we confirmed that the treatment increased miR-1246 expression on cells (Fig. 8*A*) and observed that the treated cells showed enhanced differentiation ability into osteoclasts (Fig. 8*B*,*C*). We evaluated the effects also on osteoblasts. We revealed that miR-1246 decreased during osteoblast differentiation (Fig. 8*D*). Osteoblasts treated with miR-1246 mimic showed an increase of miR-1246 (Fig. 8*E*) and *SP7* expression (Fig. 8*F*), without alteration of *RUNX2* level (Fig. 8*G*).

Discussion

Liquid biopsy and especially plasma-based EVs with the analysis of their molecular content (mRNA, miRNA and proteins) have emerged as promising diagnostic and prognostic tools for many diseases, including cancer.[8] Indeed, several diseases are characterized by EV-specific miRNA signatures and protein patterns that can be used for diagnosis. Moreover, the presence of membrane structure provides stability and allows prolonged periods of storage of EVs before analysis, making their clinical use feasible.[20]

The strength of our study is that, for the first time, it isolated EVs from postmenopausal women with different bone mass while performing a complete analysis of their cargo and their action on osteoclasts and osteoblasts. We found a correlation between EVs and T-scores; although EVs did not correlate with bone turnover markers, they exerted several effects on osteoclasts and osteoblasts. Our results revealed an increased production and release in the plasma of EVs in OP patients; the dimensions, shape, and ability to be internalized by bone cells were similar within different groups. Interestingly, the EV protein content was increased in OP and OPN groups compared to CN subjects; no significant alterations of EV protein quantification was detected between OP and OPN. This could suggest that even if osteopenia does not alter the number of circulating EVs, this condition can alter the protein levels inside EVs. Moreover, we demonstrated an increase of $RANKL^+$ EVs in plasma of OP patients, although we did not know the exact EV origins. A similar increase was also detected in plasma from patients with GSD characterized by progressive osteolysis. However, Deng et al.[21] demonstrated that osteoblast-derived EVs expressed RANKL, indicating a possible mesenchymal lineage origin for these EVs, even if RANKL is widely produced also by T lymphocytes[22] and dendritic cells.[21]

In line with Xie et al., we demonstrated the ability of OP EVs to induce the differentiation of control PBMCs.[23] Moreover, OP EVs were able to stimulate bone resorption activity of HD mature osteoclasts. Interestingly, although OPN EVs failed to stimulate bone erosion, they enhanced the expression of osteoclast function and activity genes. These results suggest a role of OPN EVs in the primer of the osteolytic disease.

As regards osteoblastogenesis, we observed that OP EVs had a specific inhibitory effect on MSCs induced to differentiate into osteoblasts, as also revealed by Xie et al.[23]; instead, on mature osteoblasts they had a stimulatory effect on the expression of osteoblast gene, as *SP7* and *RANKL*, establishing high bone turnover condition.

To evaluate the cargo of EVs and better investigate which molecules could be involved in the development of osteoporosis, we performed EV miRNome and proteomic analysis. Plasma-derived miRNAs have been investigated and are recognized as modulators of skeletal remodeling[24]; however, miRNAs found within the EVs are less studied, and their function is still debated.[25]

Among the downregulated EV-miRNAs, the analysis revealed miR-1224-5p that targets tetraspanin 5, highly expressed by osteoclasts and important for osteoclast activity,[26] and miR-193b-5p, with unknown functions in bone, that targets bone morphogenetic protein 2 (BMP2), one of the most potent osteoinductive cytokines.[27] Within the most upregulated EV-miRNAs, miR-1246 could have a role in increased osteoclast formation[28]; indeed, in our recently published paper, we demonstrated that this miRNA is upregulated during osteoclast differentiation.[16] In this study we showed that the treatment of HD osteoclast precursors with miR-1246 mimic stimulated osteoclastogenesis. Moreover, we revealed that miR-1246 was downregulated during osteoblast differentiation and the treatment with miR-1246 mimick upregulated *SP7* expression, suggesting a relevant role of miR-1246 in bone remodeling activity.

We also analyzed the involvement of this miRNA in patients affected by GSD, a very rare disorder characterized by progressive osteolysis and angiomatous lesions.[29] We performed osteoclast cultures from patients' PBMCs and observed an increase in osteoclast differentiation, activity, and miR-1246 expression; interestingly, an increase in miR-1246 was revealed in circulating exosomes of GSD patients, suggesting that this miRNA could be associated with increased bone resorption. If high levels of vesicular miR-1246 are revealed in other pediatric and adult patients with bone loss diseases, this could be an important biomarker of bone erosion.

The modulated EV-miRNAs in OP and osteopenic patients compared to CN EV-miRNAs are related to osteoclast differentiation (GO:0030316), IL-13 production (GO:0032656), and regulation of the canonical Wingless and int-1 (WNT) pathway (GO:0090263), highlighting a possible role both on osteoclasts and on osteoblasts.

In our analysis, the comparison from OPN and CN EV-miRNAs identified miR-184 as the most downregulated; the modulation of this miRNA could represent the first sign of the presence of osteolytic disease. So far, this small RNA was investigated in osteosarcoma cells but not in healthy bone cells.[30,31]

In the same group of analysis, the most upregulated miRNA is miR-137; its overexpression is associated with altered risk of fractures in patients with osteoporosis[32]; hence, the presence of this miRNA in OPN EVs could represent a prognostic tool for the progression of the disease.

The proteomic analysis of EVs revealed that patients with osteoporosis did not express von Willebrand factor (VWF) and are characterized by reduced levels of fibrinogen. The interplay between coagulation factors and bone remodeling is the subject of investigation since the characterization of the effects of coagulation factors on bone cells will be important to understand the skeleton-related events associated with a specific disease such as hemophilia.[33] Furthermore, population studies suggest that patients with hemophilia and von Willebrand disease characterized by defective VWF production have an increased risk of fractures and lower bone mineral density and that this relationship is proportional to the degree of the

factor deficiency.[34,35] Indeed, both animal models and clinical observations suggest that coagulation factor deficiencies contribute to bone loss.[36]

The role of fibrinogen in bone remodeling and bone disease is still under investigation; in 2016 Chen et al. performed a study on 41 perimenopausal women revealing an inverse correlation between fibrinogen and bone mineral density.[37] At the same time, in vitro experiments demonstrated that fibrinogen had a dual effect on osteoclast formation from murine bone marrow cultures. Indeed, when present early in the process of osteoclast formation, it inhibits osteoclastogenesis but causes a modest but significant increase when added later.[38]

Another important protein found in the EVs of patients with low bone mass is apolipoprotein AI, which is the major apolipoprotein of HDL, and in bone remodeling activity it is able to regulate osteoblast function without affecting osteoclasts. Indeed, ApoA1 knockout mice are characterized by reduced bone mass attributed primarily to suppressed osteoblastic bone synthesis and not to increased osteoclastic bone degradation.[39] Interestingly, our in vitro experiments demonstrated that mature osteoblasts treated with EVs isolated from OP patients revealed increased osterix expression.

Regarding the differential expression analysis of proteins in EVs between the groups, we found reduced levels of vitronectin in OP EVs compared to CN and OPN EVs. Vitronectin is a glycoprotein present in serum, extracellular matrix, and bone, and it regulates many physiological processes, including cell attachment, spreading, and migration.[40] Interestingly, Min et al. showed that a vitronectin-derived peptide promotes osteoblast differentiation and activity and concomitantly restrains osteoclast differentiation and resorptive function.[41]

Our study had the limitation that the exact origin of serum EV analyzed is uncertain, although it might be osteoblast-derived EVs because they express RANKL or may also be produced by T lymphocytes and dendritic cells.

In conclusion, we demonstrated in a comprehensive analysis the action of EVs on both osteoclastogenesis and osteoblastogenesis, based on different cargos of proteins and miRNAs in OP compared to OPN and CNs. Further studies are needed that have as their long-term aim to identify $RANKL^+$ EVs and vesicular miR-1246 as new diagnostic, prognostic, and therapeutic tools for diseases characterized by bone loss.

Acknowledgments

This study was supported by a SIMI grant to JP, a Sapienza grant for research project to SM (RM11715C59E67995), with the unconditional support of Sandoz to SM, the Ricerca Finalizzata Ministero della Salute GR-2019-12370244 to ADF, Million Dollar Bike Ride Grant Program, Orphan Disease Center, University of Pennsylvania #MDBR-17-116-GLA/GSD59 to ADF and AB, Italian Ministry of Health RCR-2021-23671217 project under the the Italian Musculoskeletal Apparatus Network RAMS to RMT, and by grants from the Italian Ministry of Health to ADF. MR is supported by Fondazione Veronesi Post-Doctoral Fellowship. Open Access Funding provided by Universita degli Studi di Roma La Sapienza within the CRUI-CARE Agreement.

Conflict of Interest

The authors declare no conflict of interest.

Data Availability Statement

The data that support the findings of this study are available from the corresponding author upon reasonable request.

Author Contributions

Jessica Pepe: Conceptualization; data curation; formal analysis; funding acquisition; investigation; supervision; writing – original draft; writing – review and editing. **Michela Rossi:** Conceptualization; data curation; formal analysis; investigation; writing – original draft; writing – review and editing. **Giulia Battafarano:** Investigation; writing – review and editing. **Pamela Vernocchi:** Data curation; formal analysis; investigation; writing – original draft; writing – review and editing. **Federica Conte:** Data curation; formal analysis; investigation; writing – review and editing. **Valeria Marzano:** Investigation; writing – review and editing. **Eda Mariani:** Investigation; writing – review and editing. **Stefano Levi Mortera:** Investigation; writing – review and editing. **Cristiana Cipriani:** Investigation; writing – review and editing. **Ippolita Rana:** Investigation; writing – review and editing. **Paola Sabrina Buonuomo:** Investigation; writing – review and editing. **Andrea Bartuli:** Funding acquisition; investigation; writing – review and editing. **Viviana De Martino:** Investigation; writing – review and editing. **Simone Pelle:** Investigation; writing – review and editing. **Luisa Pascucci:** Investigation; writing – review and editing. **Renato Maria Toniolo:** Funding acquisition; investigation; writing – review and editing. **Lorenza Putignani:** Investigation; writing – review and editing. **Salvatore Minisola:** Funding acquisition; project administration; supervision; writing – original draft; writing – review and editing. **Andrea Del Fattore:** Conceptualization; data curation; formal analysis; funding acquisition; methodology; supervision; writing – original draft; writing – review and editing.

References

1. Cocucci E, Racchetti G, Meldolesi J. Shedding microvesicles: artefacts no more. Trends Cell Biol. 2009;19(2):43-51.
2. Raposo G, Stoorvogel W. Extracellular vesicles: exosomes, microvesicles, and friends. J Cell Biol. 2013;200(4):373-383.
3. Mathivanan S, Ji H, Simpson RJ. Exosomes: extracellular organelles important in intercellular communication. J Proteomics. 2010; 73(10):1907-1920.
4. van der Pol E, Boing AN, Harrison P, Sturk A, Nieuwland R. Classification, functions, and clinical relevance of extracellular vesicles. Pharmacol Rev. 2012;64(3):676-705.
5. Rossi M, Battafarano G, D'Agostini M, Del Fattore A. The role of extracellular vesicles in bone metastasis. Int J Mol Sci. 2018;19(4):1-13.
6. Thery C, Ostrowski M, Segura E. Membrane vesicles as conveyors of immune responses. Nat Rev Immunol. 2009;9(8):581-593.
7. Bernardi S, Balbi C. Extracellular vesicles: from biomarkers to therapeutic tools. Biology. 2020;9(9):1-6.
8. Ciferri MC, Quarto R, Tasso R. Extracellular vesicles as biomarkers and therapeutic tools: from pre-clinical to clinical applications. Biology. 2021;10(5):1-14.
9. Huynh N, VonMoss L, Smith D, et al. Characterization of regulatory extracellular vesicles from osteoclasts. J Dent Res. 2016;95(6): 673-679.
10. Ge M, Ke R, Cai T, Yang J, Mu X. Identification and proteomic analysis of osteoblast-derived exosomes. Biochem Biophys Res Commun. 2015;467(1):27-32.

11. Qin Y, Sun R, Wu C, Wang L, Zhang C. Exosome: a novel approach to stimulate bone regeneration through regulation of osteogenesis and angiogenesis. Int J Mol Sci. 2016;17(5):1-12.
12. Schmidt JR, Kliemt S, Preissler C, et al. Osteoblast-released matrix vesicles, regulation of activity and composition by sulfated and non-sulfated Glycosaminoglycans. Mol Cell Proteomics. 2016;15(2):558-572.
13. Wang J, Faict S, Maes K, et al. Extracellular vesicle cross-talk in the bone marrow microenvironment: implications in multiple myeloma. Oncotarget. 2016;7(25):38927-38945.
14. Rossi M, Rana I, Buonuomo PS, et al. Stimulation of Treg cells to inhibit Osteoclastogenesis in Gorham-Stout disease. Front Cell Dev Biol. 2021;9:706596.
15. Momen-Heravi F. Isolation of extracellular vesicles by ultracentrifugation. Methods Mol Biol. 2017;1660:25-32.
16. Rossi M, Rana I, Buonuomo PS, et al. Dysregulated miRNAs in bone cells of patients with Gorham-Stout disease. FASEB J. 2021;35(3): e21424.
17. Duijvesz D, Burnum-Johnson KE, Gritsenko MA, et al. Proteomic profiling of exosomes leads to the identification of novel biomarkers for prostate cancer. PLoS One. 2013;8(12):e82589.
18. Livak KJ, Schmittgen TD. Analysis of relative gene expression data using real-time quantitative PCR and the 2(-Delta Delta C(T)) method. Methods. 2001;25(4):402-408.
19. Cheng F, Desai RJ, Handy DE, et al. Network-based approach to prediction and population-based validation of in silico drug repurposing. Nat Commun. 2018;9(1):2691.
20. Corrado C, Raimondo S, Chiesi A, Ciccia F, De Leo G, Alessandro R. Exosomes as intercellular signaling organelles involved in health and disease: basic science and clinical applications. Int J Mol Sci. 2013;14(3):5338-5366.
21. Deng L, Wang Y, Peng Y, et al. Osteoblast-derived microvesicles: a novel mechanism for communication between osteoblasts and osteoclasts. Bone. 2015;79:37-42.
22. Kawai T, Matsuyama T, Hosokawa Y, et al. B and T lymphocytes are the primary sources of RANKL in the bone resorptive lesion of periodontal disease. Am J Pathol. 2006;169(3):987-998.
23. Xie Y, Gao Y, Zhang L, Chen Y, Ge W, Tang P. Involvement of serum-derived exosomes of elderly patients with bone loss in failure of bone remodeling via alteration of exosomal bone-related proteins. Aging Cell. 2018;17(3):e12758.
24. Liu J, Dang L, Wu X, et al. microRNA-mediated regulation of bone remodeling: a brief review. JBMR Plus. 2019;3(9):e10213.
25. Li QC, Li C, Zhang W, Pi W, Han N. Potential effects of exosomes and their MicroRNA carrier on osteoporosis. Curr Pharm Des. 2022;28(11):899-909.
26. Zhou J, Fujiwara T, Ye S, Li X, Zhao H. Downregulation of notch modulators, tetraspanin 5 and 10, inhibits osteoclastogenesis in vitro. Calcif Tissue Int. 2014;95(3):209-217.
27. Nguyen V, Meyers CA, Yan N, Agarwal S, Levi B, James AW. BMP-2-induced bone formation and neural inflammation. J Orthop. 2017;14(2):252-256.
28. de Vries TJ, Schoenmaker T, Beertsen W, van der Neut R, Everts V. Effect of CD44 deficiency on in vitro and in vivo osteoclast formation. J Cell Biochem. 2005;94(5):954-966.
29. Rossi M, Buonuomo PS, Battafarano G, et al. Dissecting the mechanisms of bone loss in Gorham-stout disease. Bone. 2020;130:115068.
30. Lin BC, Huang D, Yu CQ, et al. MicroRNA-184 modulates doxorubicin resistance in osteosarcoma cells by targeting BCL2L1. Med Sci Monit. 2016;22:1761-1765.
31. Li C, Duan G, Feng Y. Downregulation of miR-184 facilitates osseous differentiation in periodontal ligament stem cells by modulating nuclear factor I-C. J Dent Sci. 2021;16(2):668-675.
32. Liu X, Xu X. MicroRNA-137 dysregulation predisposes to osteoporotic fracture by impeding ALP activity and expression via suppression of leucine-rich repeat-containing G-protein-coupled receptor 4 expression. Int J Mol Med. 2018;42(2):1026-1033.
33. Baud'huin M, Duplomb L, Teletchea S, et al. Factor VIII-von Willebrand factor complex inhibits osteoclastogenesis and controls cell survival. J Biol Chem. 2009;284(46):31704-31713.
34. Gay ND, Lee SC, Liel MS, Sochacki P, Recht M, Taylor JA. Increased fracture rates in people with haemophilia: a 10-year single institution retrospective analysis. Br J Haematol. 2015;170(4):584-586.
35. Mansouritorghabeh H, Rezaieyazdi Z. Bone density status in bleeding disorders: where are we and what needs to be done? J Bone Metab. 2017;24(4):201-206.
36. Chapin JV. Willebrand disease in the elderly: clinical perspectives. Clin Interv Aging. 2018;13:1531-1541.
37. Chen JT, Kotani K. Inverse correlation between fibrinogen and bone mineral density in women: preliminary findings. J Formos Med Assoc. 2016;115(1):54-56.
38. Ke K, Kim WK, Sul OJ, et al. Elevation of fibrinogen due to loss of ovarian function enhances Actin ring formation and leads to increased bone resorption. Am J Physiol Endocrinol Metab. 2012;303(11): E1296-E1303.
39. Blair HC, Kalyvioti E, Papachristou NI, et al. Apolipoprotein A-1 regulates osteoblast and lipoblast precursor cells in mice. Lab Invest. 2016;96(7):763-772.
40. Date K, Sakagami H, Yura K. Regulatory properties of vitronectin and its glycosylation in collagen fibril formation and collagen-degrading enzyme cathepsin K activity. Sci Rep. 2021;11(1):12023.
41. Min SK, Kang HK, Jung SY, Jang DH, Min BM. A vitronectin-derived peptide reverses ovariectomy-induced bone loss via regulation of osteoblast and osteoclast differentiation. Cell Death Differ. 2018; 25(2):268-281.